Optimal Pulse Sequence for Ferumoxides-Enhanced MR Imaging Used in the Detection of Hepatocellular Carcinoma: A Comparative Study Using Seven Pulse Sequences

Seung Hoon Kim, MD[1]
Dongil Choi, MD[1]
Jae Hoon Lim, MD[1]
Won Jae Lee, MD[1]
Hyun-Jung Jang, MD[1]
Hyo Keun Lim, MD[1]
Soon Jin Lee, MD[1]
Jae Min Cho, MD[1]
Seung Kwon Kim, MD[1]
Gab Chul Kim, MD[1,2]

Index terms:
Liver neoplasms, MR
Iron
Magnetic resonance (MR), contrast enhancement
Magnetic resonance (MR), comparative studies
Receiver operating characteristic (ROC)

Korean J Radiol 2002;3:87-97
Received October 11, 2001; accepted after revision March 6, 2002.

[1]Department of Radiology, Samsung Medical Center, Sungkyunkwan University School of Medicine; [2]Department of Radiology, Ulsan Boram Hospital

Address reprint requests to:
Seung Hoon Kim, MD, Department of Radiology, Samsung Medical Center, Sungkyunkwan University School of Medicine, 50 Ilwon-dong, Kangnam-gu, Seoul 135-710, Korea.
Telephone: (822) 3410-2518
Fax: (822) 3410-0084
e-mail: shkim@smc.samsung.co.kr

Objective: To identify the optimal pulse sequence for ferumoxides-enhanced magnetic resonance (MR) imaging in the detection of hepatocelluar carcinomas (HCCs).

Materials and Methods: Sixteen patients with 25 HCCs underwent MR imaging following intravenous infusion of ferumoxides. All MR studies were performed on a 1.5-T MR system, using a phased-array coil. Ferumoxides (Feridex IV) at a dose of 15 μmol/Kg was slowly infused intravenously, and axial images of seven sequences were obtained 30 minutes after the end of infusion. The MR protocol included fast spin-echo (FSE) with two echo times (TR3333–8571/TE18 and 90-117), single-shot FSE (SSFSE) with two echo times (TR∞/TE39 and 98), T2*-weighted gradient-recalled acquisition in the steady state (GRASS) (TR216/TE20), T2*-weighted fast multiplanar GRASS (FMPGR) (TR130/TE8.4–9.5), and T2*-weighted fast multiplanar spoiled GRASS (FMPSPGR) (TR130/TE8.4–9.5). Contrast-to-noise ratios (CNRs) of HCCs determined during the imaging sequences formed the basis of quantitative analysis, and images were qualitatively assessed in terms of lesion conspicuity and image artifacts. The diagnostic accuracy of all sequences was assessed using receiver operating characteristic (ROC) analysis.

Results: Quantitative analysis revealed that the CNRs of T2*-weighted FMPGR and T2*-weighted FMPSPGR were significantly higher than those of the other sequences, while qualitative analysis showed that image artifacts were prominent at T2*-weighted GRASS imaging. Lesion conspicuity was statistically significantly less clear at SSFSE imaging. In term of lesion detection, T2*-weighted FMPGR, T2*- weighted FMPSPGR, and proton density FSE imaging were statistically superior to the others.

Conclusion: T2*-weighted FMPGR, T2*- weighted FMPSPGR, and proton density FSE appear to be the optimal pulse sequences for ferumoxides-enhanced MR imaging in the detection of HCCs.

Ferumoxides, superparamagnetic iron oxide particles coated with dextran, is a tissue-specific magnetic resonance (MR) imaging contrast agent used for the detection of hepatic tumors. Particulate substances administered intravenously are cleared by phagocytosis of the reticuloendothelial system, including the Kupffer cells of the liver, substantially shortening T2 of liver tissue (1, 2). Most focal hepatic lesions, particularly malignant tumors, are devoid of Kupffer cells, and ferumoxides improves contrast between lesions and liver tissue (3–5). In a recent study, the conspicuity of nodular lesions in cirrhotic liver correlated closely with differences in the number of Kupffer cells between liver parenchyma and nodular lesions (6).

Computed tomography during arterial portography (CTAP) is considered a highly sensitive imaging modality for the preoperative detection of hepatic malignancy, with

reported sensitivities ranging from 81 to 93% (7–10). Unfortunately, CTAP, despite its high sensitivity to the presence of lesions, has major disadvantages: an invasive procedure that necessitates angiography, and a high false-positive rate (11). Ferumoxides-enhanced MR imaging has been increasingly used for the detection of focal hepatic lesions, and the initial results have been encouraging (12–18). T2-weighted spin-echo (SE) and T2*-weighted gradient-echo (GRE) sequences are regarded optimal for the detection of primary and secondary hepatic malignancies at ferumoxides-enhanced MR imaging (1, 12, 15, 19–24). To our knowledge, however, there have been few studies involving the use of various pulse sequences such as newly developed breath-hold, fast MR imaging techniques such as single-shot fast SE (SSFSE), fast multiplanar gradient-recalled acquisition in the steady state (GRASS) without preparation pulses (FMPGR), and fast multiplanar spoiled GRASS (FMPSPGR) (25, 26).

The purpose of this study was to identify the optimal pulse sequence for the detection of hepatocelluar carcinoma (HCC) at ferumoxides-enhanced MR imaging.

MATERIALS AND METHODS

Patients

Between April and August 1999, 22 consecutive patients underwent ferumoxides-enhanced MR imaging to assess known or suspected focal liver lesions. The criteria for inclusion in this study were as follows: HCC was depicted at contrast-enhanced CT, lesions were distributed in such a way that they were resectable, and the patient was considered suitable for curative hepatic resection. On this basis, five patients were excluded because HCCs were absent (metastatic adenocarcinoma was found in two, and each of cholangiocarcinoma, hepatic adenoma, and hemangioma in one), and one other because HCCs were distributed diffusely. The remaining 16 patients, 14 men and 2 women ranging in age from 35 to 66 (mean, 51) years, with 25 HCCs (diameter, 3–140 [mean, 41] mm) in 24 hepatic segments comprised our final study group. Ferumoxides-enhanced MR imaging was not performed where patients were pregnant, showed severe renal failure, or were allergic to dextran-based drugs. The study was approved by the institutional review board, and written informed consent was obtained from all patients.

For 19 HCCs in 11 patients, diagnosis was based on the histopathological findings of surgery; for two, on those of US-guided percutaneous needle biopsy; and for the remaining four, the basis of confirmation was an elevated serum α-fetoprotein level (over 200 ng/mL) and characteristic helical CT findings. Thirteen patients in the study had liver cirrhosis as a result of hepatitis B (n=12), or hepatitis C (n=1), while the remaining three had hepatitis B without cirrhosis. In order to evaluate hepatic segments which according to the findings of ferumoxides-enhanced MR imaging were HCC-free, follow-up radiologic examinations (contrast-enhanced CT or gadolinium-enhanced MR imaging) were performed no less than 12 months later. HCC did not develop in those segments during the follow-up period.

MR Imaging Examinations

All MR examinations were performed on a 1.5-T MR imager (Horizon, GE Medical Systems, Milwaukee, Wis., U.S.A.) using a phased-array coil. Two respiratory-triggered FSE sequences (TR3333–8571/TE18 and 90–117/ETL12/NEX2/fat sat.), four breath-hold sequences (proton density SSFSE [TR∞/TE39/NEX0.5], T2-weighted SSFSE [TR∞/TE98/NEX0.5], FMPGR [TR130/TE8.4-9.5/flip angle 30°], and FMPSPGR [TR130/TE8.4–9.5/flip angle 30°]), and the GRASS sequence (TR216/TE20/flip angle 60°) were performed using the parameters shown in Table 1. Transverse sections were obtained with a rectangular field of view (six-eight), a slice thickness of 6–8 mm, and an interslice gap of 2 mm. To minimize motion artifact during gradient-echo sequences, saturation bands superior and inferior to the imaging volume were applied to all sequences. Fat saturation was used during proton density and T2-weighted FSE and SSFSE sequences.

The patients underwent respiratory-triggered proton density and T2-weighted FSE imaging, with repetition times varying between 3,333 and 8,571, and between 3,240 and 8,620 msec, according to the period of the respiratory cycle. At T2*-weighted FMPSPGR and FMPGR, multiple sections were obtained in an interleaved fashion, and the whole liver was covered with 20 sections using two breath-holds.

Ferumoxides (Feridex IV; Advanced Magnetics Inc., Cambrige, Mass., U.S.A.) at a dose of 15 μmol Fe/Kg was diluted in 100 ml of 5% glucose solution and administrated intravenously through an in-line 5-μm specific filter over a 30-minute period. MR images were obtained 30 minutes after the end of infusion.

Quantitative Imaging Analysis

The images obtained during each of the seven pulse sequences were quantitatively analysed using operator-defined region-of-interest (ROI) measurements of the mean signal intensity of liver parenchyma, lesions, and background noise. For the measurement of liver signal, ROIs were set in areas devoid of focal changes in signal intensity, large vessels, and prominent artifact. If more than one

HCC was present, the largest representative lesion was identified and measured at all sequences. For liver lesions, circular or ovoid ROIs were drawn to encompass as much of the lesion as possible. Noise was measured on each image using ROIs positioned just ventral to the right anterior abdominal wall; areas with the most prominent ghost were not included. ROIs were drawn electrically, and were larger than 256 mm^2 in the liver, 45 mm^2 in lesions, and 846 mm2 in the noise area; they were drawn three times in each place and mean values were obtained. The lesion-to-liver contrast-to-noise ratio (CNR) was calculated using the following formula: (signal intensity $_{lesion}$ - signal intensity $_{liver}$)/standard deviation of background noise. Lesion-to-liver CNR was compared statistically using Wilcoxon's signed ranks test.

Qualitative Imaging Analysis

Two readers unaware of the patients' clinical data assessed the image quality obtained during each of the seven MR sequences. Each reader graded image quality as unacceptable, poor, fair, good, or excellent (with numerical scores of 1, 2, 3, 4, or 5, respectively) with regard to lesion conspicuity and image artifacts (5 = absent). Inter-reader agreement was assessed using a κ statistic: a κ score of more than 0.60 was taken to indicate substantial to excellent agreement (27). Discrepancies were resolved by consensus between the readers, and the final ranking data based on consensual interpretations were compared by means of Wilcoxon's signed ranks test.

ROC Analysis

All MR images of the 16 patients were randomized and reviewed independently by three readers experienced in MR imaging of the liver. For each pulse sequence, they recorded the number, size, and segmental location of HCCs. The name, age, identification number and imaging parameters of each patient were masked to minimize learning bias, and MR images of each pulse sequence were reviewed on a segment-by-segment basis during sessions separated by two weeks. To prevent mislocation of the lesion by the readers, hepatic segments were drawn directly by the study coordinator according to Couinaud's numbering system. A total of 128 hepatic segments were reviewed, including 24 segments with 25 HCCs. The readers scored each image for the presence or absence of HCCs and assigned one of five confidence levels, as follows: 1 = definitely or almost definitely absent, 2 = probably absent, 3 = possibly present, 4 = probably present, 5 = definitely or almost definitely present. When a lesion was located in two or more segments, the readers were asked to consider only the segment mainly involved and to assess the possibility of another lesion in the other segment. A binomial ROC curve was fitted to each reader's confidence rating using a maximum-likelihood estimation. The diagnostic accuracy of each MR sequence determined by each reader was evaluated by calculating the area under the ROC curve (Az). Composite ROC curves that combined the performance of all readers into a single curve were obtained for each MR sequence, using the maximum-likelihood curve-fitting algorithm to rate the pooled data of the three readers (28, 29). The differences between MR sequences in terms of mean Az were statistically analyzed using the two-tailed Student t test. The relative sensitivity of each sequence was calculated according to the percentage of segments assigned a score of 3 or greater ('possibly present' to 'definitely present') among a total of 24 segments with HCC. Relative specificity calculations were based on the percentage of segments assigned a score of 1 or 2 among 93 segments without HCC. Using a κ statistic, inter-reader agreement regarding the detection of segments with HCC

Table 1. Sequencing Parameters for MR Imaging of the Liver

Parameter	FSE PD	FSE T2	SSFSE PD	SSFSE T2	GRASS T2*	FMPGR T2*	FMPSPGR T2*
TR (msec)	3,333–8,571	3,242–8,623	∞	∞	217	130	130
TE (msec)	17	99	39	98	20	8.5	8.5
ETL	12	12	–	–	–	–	–
Matrix (phase x frequency)	256×256	256×256	256×192	256×192	256×192	256×160	256×160
Field of view (mm)	32×24	32×24	32×24	32×24	32×24	32×24	32×24
Bandwidth (Hz per pixel)	120	120	160	160	83.3	60	60
No. of sections acquired	20	20	20	20	20	20	20
Acquisition time (sec)	225	241	23	26	168	41	41
No. of signals acquired	1	1	1	1	1	1	1
Mode of signal acquired	Multisection	Multisection	Sequential	Sequential	Multisection	Multisection	Multisection

Note.—FSE = fast spin-echo, SSFSE = single-shot FSE, GRASS = gradient recalled acquisition in the steady state, FMPGR = fast multiplanar GRASS, FMPSPGR = fast multiplanar spoiled GRASS, PD = proton density, TR = time to repeat, TE = time to echo, ETL = echo train length

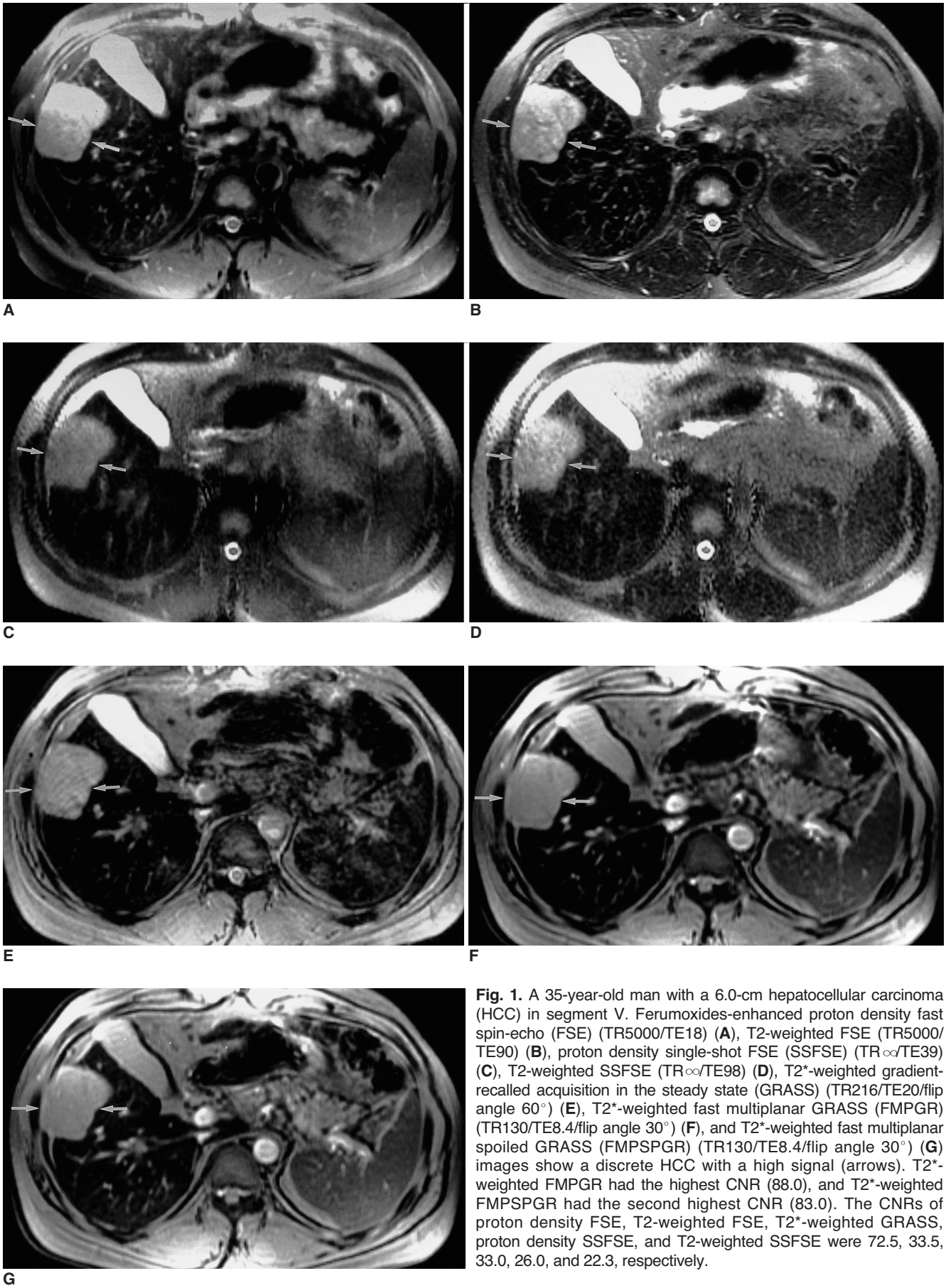

Fig. 1. A 35-year-old man with a 6.0-cm hepatocellular carcinoma (HCC) in segment V. Ferumoxides-enhanced proton density fast spin-echo (FSE) (TR5000/TE18) (**A**), T2-weighted FSE (TR5000/TE90) (**B**), proton density single-shot FSE (SSFSE) (TR∞/TE39) (**C**), T2-weighted SSFSE (TR∞/TE98) (**D**), T2*-weighted gradient-recalled acquisition in the steady state (GRASS) (TR216/TE20/flip angle 60°) (**E**), T2*-weighted fast multiplanar GRASS (FMPGR) (TR130/TE8.4/flip angle 30°) (**F**), and T2*-weighted fast multiplanar spoiled GRASS (FMPSPGR) (TR130/TE8.4/flip angle 30°) (**G**) images show a discrete HCC with a high signal (arrows). T2*-weighted FMPGR had the highest CNR (88.0), and T2*-weighted FMPSPGR had the second highest CNR (83.0). The CNRs of proton density FSE, T2-weighted FSE, T2*-weighted GRASS, proton density SSFSE, and T2-weighted SSFSE were 72.5, 33.5, 33.0, 26.0, and 22.3, respectively.

was also assessed (27). Ten hepatic cysts were diagnosed by sonography and CT, and excluded from analysis after the review was complete.

RESULTS

Quantitative Analysis

The quantitative results of assessment of mean HCC-to-liver CNR obtained during each pulse sequence are shown in Table 2. The highest CNR was achieved with breath-hold T2*-weighted FMPGR sequences (68.9 ±25.0); this ratio was statistically significantly higher than those obtained during all other sequences except breath-hold T2*-weighted FMPSPGR ($p < .05$) (Fig. 1). The ratio obtained during this sequence was the second highest and was statistically significantly higher than those recorded during the sequences ranked 4 to 7 ($p < .05$).

Qualitative Analysis

Table 3 summarizes the results of qualitative analysis for each sequence. HCCs were statistically significantly clearer at proton density and T2-weighted FSE, and at all three

Table 2. HCC-to-Liver CNRs for Ferumoxides-Enhanced MR Imaging Using Various Pulse Sequences

Sequence	HCC-to-Liver CNR	Rank
FSE PD	35.0 ±26.8	3
FSE T2	27.3 ±15.0	4
SSFSE PD	19.3 ±12.7	6
SSFSE T2	17.7 ±12.9	7
GRASS T2*	25.2 ±13.6	5
FMPGR T2*	68.9 ±25.0	1
FMPSPGR T2*	51.7 ±29.4	2

Note.— Values were given as means ±SDs. There were significant ($p < .05$) differences in HCC-to-liver CNR between the following comparisons (numbers indicate rank): the sequence ranked 1 vs. those ranked 3–7, and the sequence ranked 2 vs. those ranked 4–7.

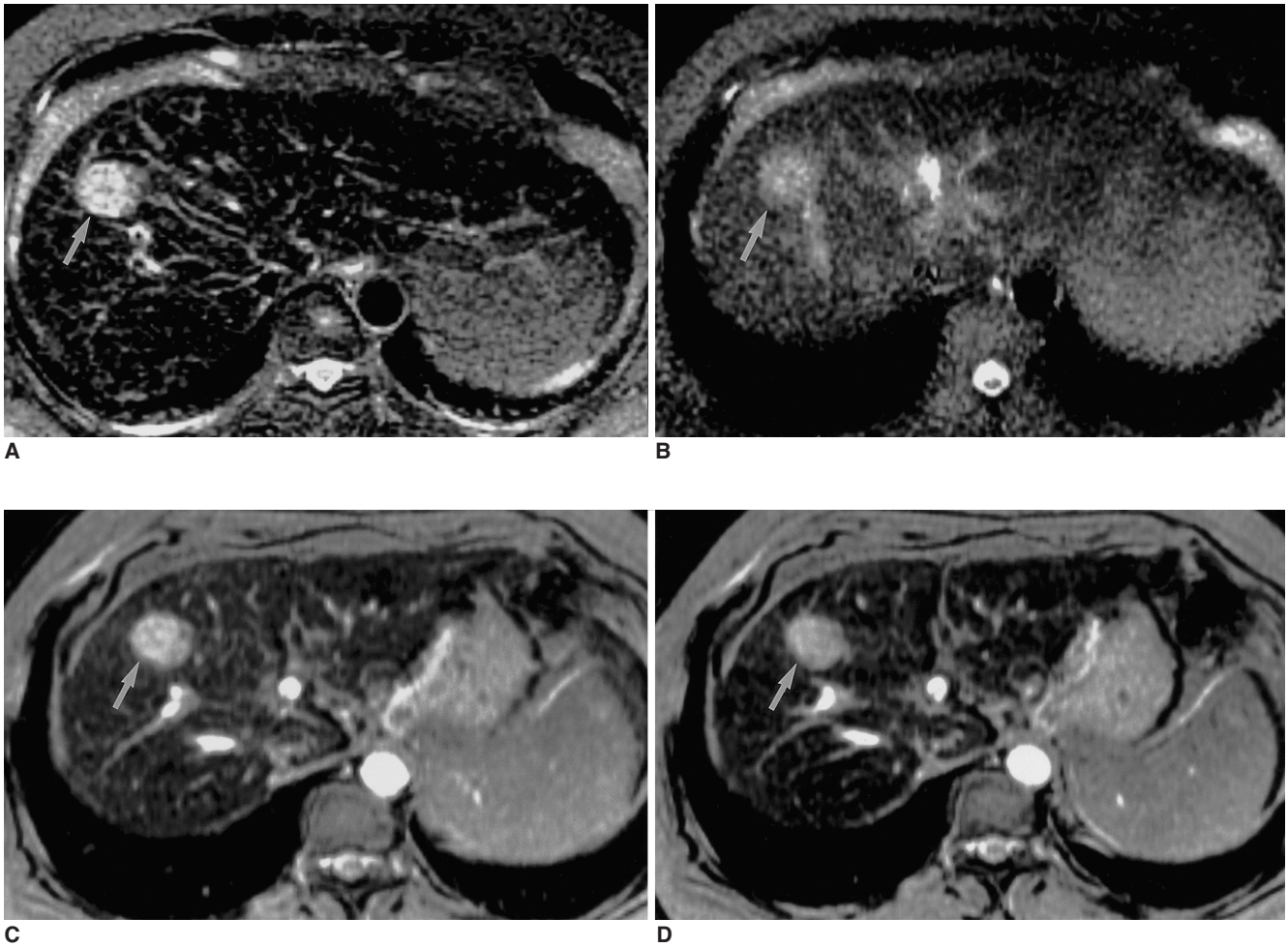

Fig. 2. A 41-year-old woman with a 2.8-cm HCC in segment VIII. T2-weighted FSE (**A**), T2-weighted SSFSE (**B**), T2*-weighted FMPGR (**C**), and T2*-weighted FMPSPGR (**D**) images depict a high-signal HCC (arrow). The highest CNR (76.0) was seen at T2*-weighted FMPGR imaging, while lesion conspicuity was significantly lower at SSFSE than at other sequences.

types of gradient-echo imaging than at the two SSFSE sequences (Fig. 2).

T2*-weighted GRASS imaging depicted imaging artifacts more prominently than did the other six sequences, and image interpretation was interfered with in 63% of cases (10/16) (Table 3). T2*-weighted GRASS imaging demonstrated pulsation artifacts due to heartbeat in all 16 patients (Fig. 3), motion-related artifacts were evident at proton density and T2-weighted FSE imaging in 63% (10/16) and 50% (8/16), respectively. All T2*-weighted FMPGR

Table 3. Lesion Conspicuity and Imaging Artifacts for Ferumoxides-Enhanced MR Imaging Using Various Pulse Sequences

Sequence	Lesion Conspicuity	Rank	Imaging Artifact	Rank
FSE PD	4.61 ±0.89	4	4.00 ±0.52	5
FSE T2	4.74 ±0.54	2	4.18 ±0.66	3
SSFSE PD	3.74 ±1.10	6	4.25 ±0.58	2
SSFSE T2	3.61 ±1.03	7	4.56 ±0.51	1
GRASS T2*	4.57 ±0.95	5	3.25 ±0.58	7
FMPGR T2*	4.78 ±0.52	1	4.00 ±0.00	5
FMPSPGR T2*	4.74 ±0.62	2	4.06 ±0.25	4

Note.— Values were given as means ±SDs. There were significant (p<.05) differences between the following comparisons (numbers indicate rank): the sequences ranked 1–5 vs. those ranked 6, 7 for lesion conspicuity; the sequence ranked 1 vs. those ranked 2–7 for imaging artifacts; and the sequence ranked 7 vs. those ranked 2–5 for imaging artifacts.

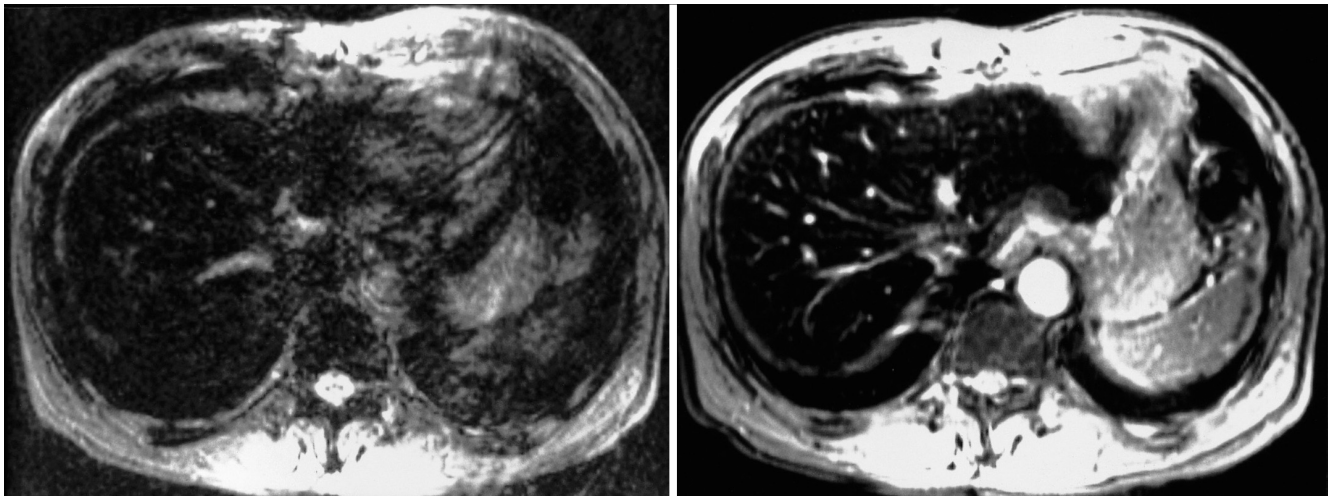

A **B**

C

Fig. 3. A 59-year-old man with an HCC (not shown). Ferumoxides-enhanced T2*-weighted GRASS (**A**), T2*-weighted FMPGR (**B**), and T2*-weighted FMPSPGR (**C**) images show significant pulsation artifacts due to the heart and aorta. Particularly at T2*-weighted GRASS imaging, the heartbeat artifact may interfere with depiction of the lesion in the left hepatic lobe.

and FMPSPGR imaging showed ghost artifacts due to aortic pulsation in the phase-encoding direction, but proton density and T2-weighted SSFSE imaging revealed no such artifacts. Overall, the imaging artifacts of the six sequences other than T2*-weighted GRASS were comparable. The lowest κ score for interobserver agreement between readers was 0.712, and was for proton density SSFSE imaging which depicted lesion conspicuity. Hence, agreement regarding lesion conspicuity and imaging artifacts was considered substantial to excellent for all sequences.

ROC Analysis

Table 4 shows the calculated areas under the ROC curves and the mean area determined by the three readers for each of the seven sequences. ROC curves drawn on the basis of pooled data from the three readers for each of these sequences are shown in Figure 4. With regard to lesion detection, two readers performed significantly better with the T2*-weighted FMPGR, T2*- weighted FMPSPGR, and proton density FSE sequences than the other four. One reader's interpretation of the seven sequences demonstrated no statistically significant differences in lesion detection. In terms of integrated lesion detectability on the basis of the pooled data reviewed by all observers, T2*-weighted FMPGR, T2*- weighted FMPSPGR, and proton density FSE imaging were statistically superior to those obtained using the other sequences (Fig. 5). The mean areas under the composite ROC curves of the three readers were 0.965 $\pm$0.015 for T2*-weighted FMPGR sequences, 0.964 $\pm$ 0.016 for T2*- weighted FMPSPGR, and 0.958 $\pm$0.017 for proton density FSE.

The relative sensitivities of T2*-weighted FMPGR, T2*-weighted FMPSPGR, and proton density FSE imaging were superior to those obtained using the other sequences (Table 5). Expressed as a percentage, the relative specificity of all sequences was 93 or more (Table 6). The lowest κ score for interobserver agreement was 0.690, and involved T2-weighted FSE imaging between reader 2 and reader 3. Agreement was thus considered substantial to excellent for all sequences.

DISCUSSION

The acquisition of high-quality images in the shortest possible time has been a major field of investigation in MR imaging of the liver. According to recent reports, ferumoxides-enhanced MR imaging is useful for the detection of hepatic tumors, including metastasis (5, 12, 15, 22) and HCCs (3–5, 24), and investigators have also claimed that it is as accurate as CTAP for detecting hepatic metastasis (12) or HCC (11).

T2-weighted SE and T2*-weighted GRE are accepted ferumoxides-enhanced MR imaging sequences (13, 24, 30,

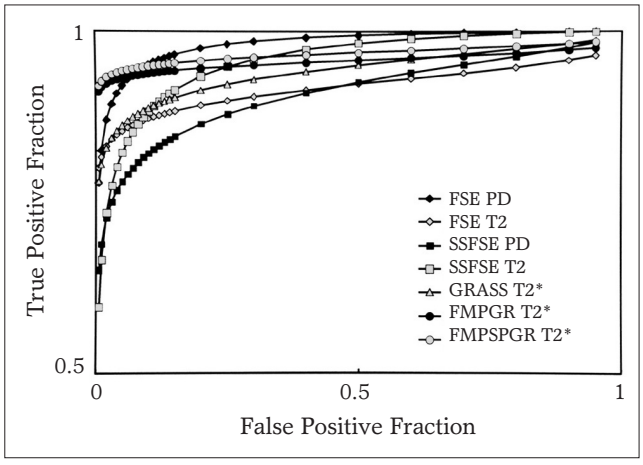

Fig. 4. Graph showing composite receiver operating characteristic (ROC) curves for pooled data reviewed by three observers. Areas under ROC curves indicate the relative accuracy with which HCCs were detected at ferumoxides-enhanced MR imaging obtained during the seven sequences. T2*-weighted FMPGR, T2*-weighted FMPSPGR, and proton density FSE were statistically superior to the other sequences. According to the three readers, the mean areas under the composite ROC curves were 0.965 $\pm$0.015 for the T2*-weighted FMPGR sequence, 0.964 $\pm$0.016 for T2*-weighted FMPSPGR, and 0.958 $\pm$0.017 for proton density FSE, respectively.

Table 4. ROC for Ferumoxides-Enhanced MR Imaging Using Various Pulse Sequences: Results for Each Reader and All Readers

Sequence	Az				Az Rank (All Readers)
	Reader 1	Reader 2	Reader 3	All Readers	
FSE PD	0.931 $\pm$0.037	0.977 $\pm$0.022	0.969 $\pm$0.025	0.958 $\pm$0.017	3
FSE T2	0.916 $\pm$0.040	0.971 $\pm$0.024	0.893 $\pm$0.045	0.924 $\pm$0.022	6
SSFSE PD	0.866 $\pm$0.049	0.959 $\pm$0.029	0.860 $\pm$0.050	0.894 $\pm$0.026	7
SSFSE T2	0.933 $\pm$0.036	0.954 $\pm$0.030	0.905 $\pm$0.042	0.928 $\pm$0.022	4
GRASS T2*	0.915 $\pm$0.040	0.950 $\pm$0.032	0.914 $\pm$0.041	0.925 $\pm$0.022	5
FMPGR T2*	0.957 $\pm$0.029	0.957 $\pm$0.029	0.979 $\pm$0.021	0.965 $\pm$0.015	1
FMPSPGR T2*	0.964 $\pm$0.016	0.955 $\pm$0.030	0.979 $\pm$0.021	0.964 $\pm$0.016	2

Note.—Values were given as means $\pm$SDs. The Az differences between sequences ranked 1-3 and those ranked 4-7 were significant (p<.05).

31). At GRE imaging after intravenous ferumoxides administration, signal loss of liver parenchyma is increased by the presence of iron oxide particles because of its greater susceptibility resulting from local field inhomogeneity (intravoxel dephasing) (21, 32). Fretz et al. (21) found that GRE imaging with long TE and a narrow flip angle was an ideal T2*-weighted sequence.

Yamamoto et al. (24) reported that HCC detection was similar at ferumoxides-enhanced T2-weighted SE and GRE imaging. In a study by Schwarz et al. (32), conventional SE

Fig. 5. A 60-year-old man with two HCCs measuring 0.6 cm and 0.3 cm in segment VIII. Ferumoxides-enhanced proton density FSE (**A**), T2-weighted FSE (**B**), T2*-weighted FMPGR (**C**), and T2*-weighted FMPSPGR (**D**) images show two discrete, high-signal HCCs (large arrow and small arrow). Proton density SSFSE (**E**) and T2-weighted SSFSE (**F**) images do not demonstrate these small lesions.

was found to be superior to FSE due to the absence of a 180° refocusing pulse. However, because FSE sequences are less sensitive to motion artifacts, and the decrease in liver signal noted at FSE is comparable to that observed at conventional SE, FSE sequences are, according to a recent report (33), clinically useful for ferumoxides imaging. Van Beers et al. (23) claimed that ferumoxides-enhanced GRE imaging was as accurate as T2-weighted SE imaging for the detection of malignant hepatic tumors and was superior for determining their segmental location. However, the optimal imaging sequence for lesion detection with ferumoxides enhancement is still open to debate.

Our results indicate that HCC-to-liver CNR was best at T2*-weighted FMPGR sequence, for which the ratio was statistically significantly higher than for all other sequences except T2*-weighted FMPSPGR. One possible reason for the lower CNR found with FSE and SSFSE imaging is that a larger matrix is used for these sequences; this contributes to the sharpness of lesion contour, but leads to low lesion-to-liver CNR. The predominance of T2*-weighted imaging is, however, thought to be caused mainly by local field inhomogeneity and the lack of a refocusing pulse (21, 32). Low CNR at T2*-weighted GRASS results from the high noise level of this sequence.

Because of poor soft-tissue resolution due to the T2 filtering effect, lesion conspicuity at SSFSE imaging was statistically significantly less clear than at other sequences. Motion-related artifacts were significantly less severe with T2-weighted and proton density SSFSE, T2*-weighted FMPGR, and T2*-weighted FMPSPGR imaging, mainly because of their short acquisition time, which allows successful breath-holding (34).

In terms of lesion-to-liver CNR, lesion conspicuity and artifacts, T2*-weighted imaging was the best sequence, though vascular structures and HCCs were similarly demonstrated with a (bright) high signal. At FSE, on the other hand, vascular structures were less bright than HCCs (Figs. 1, 2, 5).

In ROC analysis, the area under the composite ROC curve indicates performance. With regard to integrated lesion detectability, T2*-weighted FMPGR, T2*- weighted FMPSPGR, and proton density FSE imaging were statistically superior to other sequences. The difference in performance among MR sequences was more prominent for small HCCs because these can demonstrate active uptake of ferumoxides particles, which results in slight hyperinten-

Table 5. The Sensitivity of Ferumoxides-Enhanced MR Imaging Using Various Pulse Sequences for the Identification of 24 Hepatic Segments with HCC

Sequence	Numbers of Segments Assigned a Score of 3-5 among 24 Segments with HCC			
	Reader 1	Reader 2	Reader 3	All Readers
FSE PD	20 (83)	23 (96)	22 (92)	65 (90)
FSE T2	20 (83)	23 (96)	18 (75)	61 (85)
SSFSE PD	16 (67)	18 (75)	17 (71)	51 (71)
SSFSE T2	18 (75)	21 (88)	18 (75)	58 (81)
GRASS T2*	20 (83)	21 (88)	19 (79)	60 (83)
FMPGR T2*	22 (92)	22 (92)	23 (96)	67 (93)
FMPSPGR T2*	21 (88)	22 (92)	22 (92)	65 (90)

Note.—Numbers in parentheses indicate sensitivity expressed as a percentage.

Table 6. The Specificity of Ferumoxides-Enhanced MR Imaging Using Various Pulse Sequences for the Identification of 93 Hepatic Segments without HCC

Sequence	Numbers of Segments Assigned a Score of 1 or 2 among 93 Segments without HCC			
	Reader 1	Reader 2	Reader 3	All Readers
FSE PD	90 (97)	89 (96)	91 (98)	270 (97)
FSE T2	92 (99)	86 (93)	93 (100)	271 (97)
SSFSE PD	91 (98)	91 (98)	91 (98)	273 (98)
SSFSE T2	92 (99)	86 (93)	90 (97)	268 (96)
GRASS T2*	92 (99)	90 (97)	91 (98)	273 (98)
FMPGR T2*	92 (99)	92 (99)	93 (100)	277 (99)
FMPSPGR T2*	91 (98)	92 (99)	93 (100)	276 (99)

Note.—Numbers in parentheses indicate specificity expressed as a percentage.

sity, isointensity, or even hypointensity at ferumoxides-enhanced imaging (6).

Ferumoxides-enhanced MR imaging does not always facilitate differentiation between malignant tumors and benign lesions. Oudkerk et al. (13) recommended T1-weighted GRE (short TE) imaging after ferumoxides enhancement in order to detect and characterize focal liver lesions. Cysts can demonstrate low signal intensity at T1-weighted imaging, and at ferumoxides-enhanced imaging, T1-weighted sequences may permit good differentiation between malignancy and cysts. Due to the T2 effect, however, cysts can show high signal intensity at gradient-recalled echo sequences with long TE. According to Grangier et al., hemangiomas can be enhanced by shortening the T1 relaxation time at T1-weighted imaging after ferumoxides administration (35).

This study suffers certain limitations. First, while the standard of reference is the findings of histopathological analysis of 41 resected hepatic segments in 11 patients, follow-up imaging findings were used as the standard of reference for 87 unresected segments. Second, in the segments containing two hepatocelluar carcinomas or a hepatocellular carcinoma and a benign lesion (13%, n=3), segment-by-segment analysis meant that comparisons for these particular lesions could not be made. Third, it was only in the detection of HCCs that optimal pulse sequences for ferumoxides-enhanced MR imaging were evaluated: optimal sequences for the characterization of focal hepatic lesions could not be determined. Finally, unenhanced MR imaging was reported to be necessary in order to decrease the number of false-positive findings attributed to vascular structures. However, "biphasic" unenhanced and ferumoxides-enhanced MR imaging is time consuming and such unenhanced imaging is thus not obtained (36). Without unenhanced imaging, we recorded few false-positive findings.

In conclusion, our results suggest that T2*-weighted FMPGR, T2*-weighted FMPSPGR, and proton density FSE sequences after intravenous ferumoxides administration provide higher diagnostic accuracy than the other four sequences (T2-weighted SSFSE, T2*-weighted GRASS, T2-weighted FSE, and proton density SSFSE), and show higher CNRs, fewer image artifacts and better lesion conspicuity. For the detection of HCCs at ferumoxides-enhanced MR imaging, they thus appear to be the optimal pulse sequences.

References

1. Saini S, Stark DD, Hahn PF, Wittenberg J, Brady TJ, Ferrucci JT. Ferrite particles: a superparamagnetic MR contrast agent for the reticuloendothelial system. *Radiology* 1987;162:211-216
2. Stark DD, Weissleder R, Elizondo G, et al. Superparamagnetic iron oxide: clinical application as a contrast agent for MR imaging of the liver. *Radiology* 1988;168:297-301
3. Kawamori Y, Matsui O, Kadoya M, Yoshikawa J, Demachi H, Takashima T. Differentiation of hepatocellular carcinoma from hyperplastic nodules induced in rat liver with ferrite-enhanced MR imaging. *Radiology* 1992;183:65-72
4. Vogl TJ, Hammerstingl R, Schwarz W, et al. Superparamagnetic iron oxide-enhanced versus gadolinium-enhanced MR imaging for differential diagnosis of focal liver lesions. *Radiology* 1996;198:881-887
5. Paley MR, Mergo PJ, Torres GM, Ros PR. Characterization of focal hepatic lesions with ferumoxides-enhanced T2-weighted MR imaging. *AJR* 2000;175:159-163
6. Lim JH, Choi D, Cho SK, et al. Conspicuity of hepatocellular nodular lesions in cirrhotic livers at ferumoxides-enhanced MR imaging: importance of Kupffer cell number. *Radiology* 2001;220:669-676
7. Nelson RC, Chezmar JL, Sugarbaker PH, Bernardino ME. Hepatic tumors: comparison of CT during arterial portography, delayed CT, and MR imaging for preoperative evaluation. *Radiology* 1989;172:27-34
8. Heiken JP, Weyman PJ, Lee LKT, et al. Detection of focal hepatic masses: prospective evaluation with CT, delayed CT, CT during arterial portography, and MR imaging. *Radiology* 1989;171:47-51
9. Soyer P, Levesque M, Elias D, Zeitoun G, Roche A. Detection of liver metastases from colorectal cancer: comparison of intraoperative ultrasound and CTAP. *Radiology* 1992;183:531-544
10. Soyer P, Levesque M, Caudron C, Elias D, Zeitoun G, Roche A. MRI of liver metastases from colorectal cancer vs CT during arterial portography. *J Comput Assist Tomogr* 1993;17:67-74
11. Choi D, Kim SH, Lim JH, et al. Preoperative detection of hepatocellular carcinoma: ferumoxides-enhanced MR imaging versus combined helical CT during arterial portography and CT hepatic arteriography. *AJR* 2001;176:475-482
12. Seneterre E, Taourel P, Bouveir Y, et al. Detection of hepatic metastases: ferumoxides-enhanced MR imaging versus unenhanced MR imaging and CT during arterial portography. *Radiology* 1996;200:785-792
13. Oudkerk M, Heuvel AG, Wielopolski PA, Schitz PI, Rinkes IHMB, Wiggers T. Hepatic lesions: detection with ferumoxide-enhanced T1-weighted MR imaging. *Radiology* 1997;203:449-456
14. Yamamoto H, Tasuyuku Y, Yoshimatsu S, et al. Hepatocellular carcinoma in cirrhotic livers: detection with unenhanced and iron oxide-enhanced MR imaging. *Radiology* 1995;195:106-112
15. Hagspiel KD, Neidl KFW, Eichenberger AC, Weder W, Marinecek B. Detection of liver metastases: comparison of superparamagnetic iron oxide-enhanced and unenhanced MR imaging at 1.5 T with dynamic CT, intraoperative US, and percutaneous US. *Radiology* 1995;196:471-478
16. Ward J, Naik KS, Guthrie JA, Wilson D, Robinson PJ. Hepatic lesion detection: comparison of MR imaging after the administration of superparamagnetic iron oxide with dual-phase CT by using alternative-free response receiver operating characteristic analysis. *Radiology* 1999;210:459-466
17. Blakeborough A, Ward J, Wilson D, et al. Hepatic lesion detection at MR imaging: a comparative study with four sequences. *Radiology* 1997;203:759-765
18. Tanimoto A, Satoh Y, Yuasa Y, Jinzaki M, Hiramatsu K. Performance of Gd-EOB-DTPA and superparamagnetic iron oxide particles in the detection of primary liver cancer: a compara-

tive study by alternative free-response receiver operating characteristic analysis. *J Magn Reson Imaging* 1997;7:120-124
19. Ros PR, Freeny PC, Harms SE, et al. Hepatic MR imaging with ferumoxides: a multicenter clinical trial of the safety and efficacy in the detection of focal hepatic lesions. *Radiology* 1995;196:481-488
20. Winter TC, Freeny PC, Nghiem HV, et al. MR imaging with IV superparamagnetic iron oxide: efficacy in the detection of focal hepatic lesions. *AJR* 1993;161:1191-1198
21. Fretz CJ, Elizondo G, Weissleder R, Hahn PF, Stark DD, Ferrucci JT. Superparamagnetic iron oxide-enhanced MR imaging: pulse sequence of optimization for detection of liver cancer. *Radiology* 1989;172:393-397
22. Bellin MF, Zaim S, Auberton E, et al. Liver metastases: safety and efficacy of detection with superparamagnetic iron oxide in MR imaging. *Radiology* 1994;193:657-663
23. Van Beers BE, Lacrosse M, Jacques J, et al. Detection and segmental location of malignant hepatic tumors: comparison of ferumoxides-enhanced gradient-echo and T2-weighted spin-echo MR imaging. *AJR* 1997;168:713-717
24. Yamamoto H, Yamashita Y, Yoshimatsu S, et al. Hepatocellular carcinoma in cirrhotic liver: detection with unenhanced and iron oxide-enhanced MR imaging. *Radiology* 1995;195:106-112
25. Arbab AS, Ichikawa T, Araki T, et al. Detection of hepatocellular carcinoma and its metastases with various pulse sequences using superparamagnetic iron oxide (SHU-555-A). *Abdom Imaging* 2000;25:151-158
26. Kanematsu M, Itoh K, Matsuo M, et al. Malignant hepatic tumor detection with ferumoxides-enhanced MR imaging with a 1.5-T system: comparison of four imaging pulse sequences. *J Magn Reson Imaging* 2001;13:249-257
27. Landis JR, Koch GG. The measurement of observer agreement for categorical data. *Biometrics* 1977;33:150-174
28. Metz CE. Some practical issues of the experimental design and data analysis in radiological ROC studies. *Invest Radiol* 1989;24:234-245
29. Hanley JA, McNeil BJ. The meaning and use of the area under a receiver operating characteristic (ROC) curve. *Radiology* 1992;143:29-36
30. Tang Y, Yamashita Y, Arakawa A, et al. Detection of hepatocellular carcinoma arising in cirrhotic livers: comparison of gadolinium- and ferumoxides-enhanced MR imaging. *AJR* 1999;172:1547-1554
31. Ward J, Chen F, Guthrie JA, et al. Hepatic lesion detection after superparamagnetic iron oxide enhancement: comparison of five T2-weighted sequences at 1.0 T by using alternative-free response receiver operating characteristic analysis. *Radiology* 2000;214:159-166
32. Schwartz LH, Seltzer SE, Tempany CM, et al. Superparamagnetic iron oxide hepatic MR imaging: efficacy and safety using conventional and fast spin-echo pulse sequences. *J Magn Reson Imaging* 1995;5:566-570
33. Abe Y, Yamashita Y, Namimoto T, Tang Y, Takahashi M. The value of fast and ultrafast T2-weighted MR imaging sequences in hepatic enhancement with ferumoxides: comparison with conventional spin-echo sequence. *Radiat Med* 2000;18:97-105
34. Semelka RC, Kelekis NL, Thomasson D, Brown MA, Laub GA. HASTE MR imaging: description of technique and preliminary results in the abdomen. *J Magn Reson Imaging* 1996;6:698-699
35. Grangier C, Tourniaire J, Mentha G, et al. Enhancement of liver hemangiomas on T1-weighted MR SE images by superparamagnetic iron oxide particles. *J Comput Assist Tomogr* 1994;18:888-896
36. Soyer P. Will ferumoxides-enhanced MR imaging replace CT during arterial portography in the detection of hepatic metastases? Prologue to a promising future. *Radiology* 1996;201:610-611